ELSEVIER

Diamond and Related Materials 11 (2002) 1062–1067

DIAMOND AND RELATED MATERIALS

www.elsevier.com/locate/diamond

Elastic constants and structural properties of nanometre-thick diamond-like carbon films

M.G. Beghi[a], A.C. Ferrari[b,*], C.E. Bottani[a], A. Libassi[a], B.K. Tanner[c], K.B.K. Teo[b], J. Robertson[b]

[a]*Nuclear Engineering Department, Politecnico di Milano, I-20133 Milan, Italy*
[b]*Engineering Department, Cambridge University, Cambridge CB2 1PZ, UK*
[c]*Department of Physics, University of Durham, Durham DH1 3LE, UK*

Abstract

Carbon coatings of thickness down to 2 nm are needed to increase the storage density in magnetic hard disks and reach the 100-Gbits/inch^2 target. We show that the combination of surface Brillouin scattering, X-ray reflectivity and Raman spectroscopy measurements allow us to measure the mechanical and structural properties of ultra-thin tetrahedral amorphous carbon films. Densities up to 2.8 g/cm^3 are found indicating a significant sp^3 content even in the thinnest films. Surface Brillouin scattering provides the dispersion relations of surface acoustic waves and from these the elastic constants of the films. The elastic constants of 2, 4 and 8 nm-thick films are measurably different. Our results show that these ultra-thin films reach the full stiffness of tetrahedral amorphous carbons when the thickness becomes of the order of 10 nm, but even the thinnest films have a Young's modulus of at least ~100 GPa. The combination of surface sensitivity and resonant enhancement of UV Raman, with surface enhancement effects obtained by depositing the films on Al, allows the detection of the Raman spectrum, even for the thinnest films. This is the quickest non-destructive structural probe of nanometre-thick diamond-like carbon films.

Keywords: Diamond-like carbon; Brillouin scattering; X-Ray reflectivity; Raman spectroscopy

1. Introduction

Carbon coatings of thickness down to 2 nm are needed to maintain the increasing trend of storage density in magnetic hard disks and reach the 100-Gbits/inch^2 target [1,2]. The thinner the protective carbon coating, the closer the reading head can approach the magnetic part of the disk and thus, the smaller the size of the bits and the higher the bit density. For films having a thickness in the nanometre range the measurement of the elastic properties is critical. Indentation techniques become very sensitive to the substrate properties. Acoustic waves provide a clean way to measure the elastic properties. The velocities of surface acoustic waves (SAWS) can be measured by surface Brillouin scattering (SBS) [3,4]. If independent measurements of film thickness and mass density are available, the elastic constants can be derived from measured acoustic velocities. Such measurements can be performed by X-ray reflectivity (XRR). The combination of SBS and XRR measurements was used to measure the elastic constants of films in the hundreds to tens of nanometres thickness range [5,6]. Here, we show that we can push the limits of these techniques to the sub-10 nanometre range. We also show that a combination of visible and UV Raman spectroscopy can probe quickly and non-destructively the sp^3 bonding and sp^3 clustering down to the nanometre films. In particular, we report an order of magnitude enhancement of the Raman intensity for UV excitation for ultra-thin films on an evaporated Al substrate.

2. Experiment

Tetrahedral amorphous carbon (ta-C) films were deposited at floating potential using a filtered cathodic vacuum arc (FCVA) with an integrated off-plane double bend (S-bend) magnetic filter. For reference, thicker ta-C films have a particle area coverage of $<0.01\%$ and uniform cross-section, 88% sp^3 content and E_{04} gaps up to ~4 eV [7–9]. Sets of films were grown for increasing

*Corresponding author. Tel.: +44-1223-765242; fax: +44-1223-332662.
E-mail address: acf26@eng.cam.ac.uk (A.C. Ferrari).

0925-9635/02/$ - see front matter
PII: S0925-9635(01)00642-2

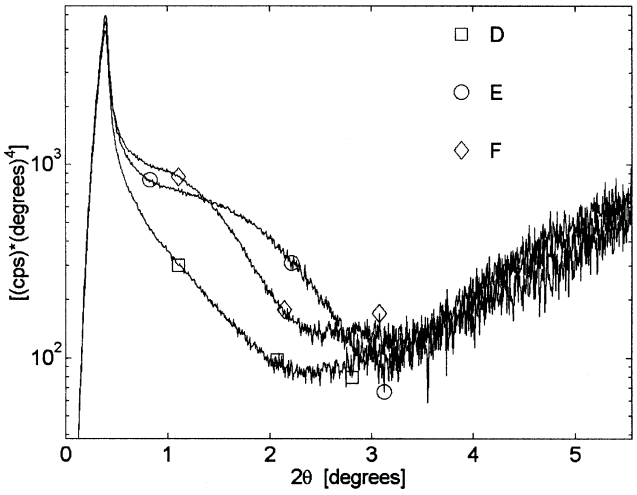

Fig. 1. Specular intensity multiplied by the fourth power of the incidence angle 2θ for the Si substrate (D) and ~2.2 (E) and ~3.5 nm (F) films, see Table 1.

deposition times on bare Si and on Si covered by thermally evaporated Al. The samples on Si and Si + Al were deposited in the same run for each deposition time. The samples on Si were used for SBS and XRR measurements, whilst both samples on Si and Si + Al were measured by multi-wavelength Raman spectroscopy.

For XRR and SBS, two sets of three samples each (A, B, C and D, E, F) are analysed here. Each set includes a bare substrate (A and D) and two ta-C films of different thickness. The 'bare' substrate is really covered with a thin layer of native oxide, due to exposure to air, with thickness (1–2 nm) comparable to the carbon films.

The thickness, density and layering of these ultra-thin samples were derived by specular XRR measurements made on a Bede GXR1 reflectometer using CuKα radiation. The data were automatically fitted to the scatter simulated from model structures using the Bede REFS-MERCURY code [9–12].

BS measurements from bulk phonons were performed to characterise the bare substrates. SBS measurements were performed with SAW propagation along the [100] direction on the (001) face of the Si substrate. The light source was a 514.5 nm Argon ion laser. The scattered light was collected without polarisation analysis by a tandem 3+3 pass high contrast interferometer of the Sandercock type [3] with a finesse of approximately 100. Unpolarized Raman spectra were acquired for 514.5 and 244 nm excitation, on two Renishaw systems optimised for visible and UV Raman measurements, respectively.

3. Results

3.1. XRR

The results for the bare Si and samples E and F are shown in Fig. 1 as reflectivity curves multiplied by the fourth power of the incidence angle, in order to enhance the visibility of low-contrast fringes [12]. The reflectivity profile from the native oxide film is clearly different from the one of samples E and F. Sample E shows only a broad fringe. For sample F, deposited for longer time, the fringe is displaced towards smaller angles, consistent with increasing thickness of the ta-C film, and a second fringe becomes visible.

The critical angle is defined by the spike in the plot. From its position the near-surface density is usually determined. However, for these ultra thin films the evanescent wave reaches the silicon substrate and the observed critical angle is mainly determined by the substrate density [12]. Simulations confirm that only for films thicker than ~20 nm the critical angle can be used reliably to measure the near-surface density [12]. Below this thickness, it is necessary to fit to the whole reflectivity curve. The results are listed in Table 1. The mean density of ~2.8 g/cm^3 is less than that of thick films, ~3.3 g/cm^3. This shows that the surface and interface layers have the effect of reducing the mean density and mean sp^3 bonding of ultra-thin films. A mean density of ~2.8 g/cm^3 would correspond to a mean sp^3 fraction of ~65%, according to the density vs. sp^3 relation of ref. [9]. The actual sp^3 content could be even higher if nano-voids would be present.

Thicker ta-C films show lower density layers at the substrate/film interface and at the external surface [9,13]. A similar three-layer model can be used to fit the XRR profiles of these ultra-thin films. We find an

Table 1
Thickness, *h*, density, ρ, and roughness, σ, derived from best-fit simulations of XRR profiles. For samples B and C both a three-layer and a single-layer model are considered. The values of *E* and *G* are obtained as 90% confidence intervals from the SBS data fit

Sample	*h* (nm)	ρ (g/cm^3)	σ (nm)	*E* (GPa)	*G* (GPa)
E	2.2	2.8	0.8	95±30	40±20
F	3.5	2.8	0.66	195±30	85±30
B (layered)	0.6/3.3/0.6	2.1/3.1/2.25	0.7		
B	4.5	2.8		220±40	100±30
C (layered)	1.5/4.8/1.8	2.5/3.1/2.3	0.5		
C	8	2.8		380±40	170±45

interface and a surface layer which have properties similar to those found for thicker films [9]: 0.5–1.5 nm thickness; and 2.0–2.5 g/cm^3 density. The intermediate layer has a higher density (3.0–3.1 g/cm^3) and a thickness increasing with the deposition time, Table 1. The existence of a less dense surface layer is due to the deposition mechanism of subsurface ion implantation (subplantation), whilst the interface layer is a mixture of Si, C and O due to the energetic C ion bombardment [9].

These results show that the measurement of a film of 2 nm thickness is quite within the capability of XRR. While the statistical precision on the best-fit parameter is sub-Ångstrom, the effective precision for the thickness measurement is 0.1 nm [13]. We considered these layers to be a single homogeneous equivalent layer in order to fit the SBS data, since we are interested in a more precise evaluation of the average properties of the films.

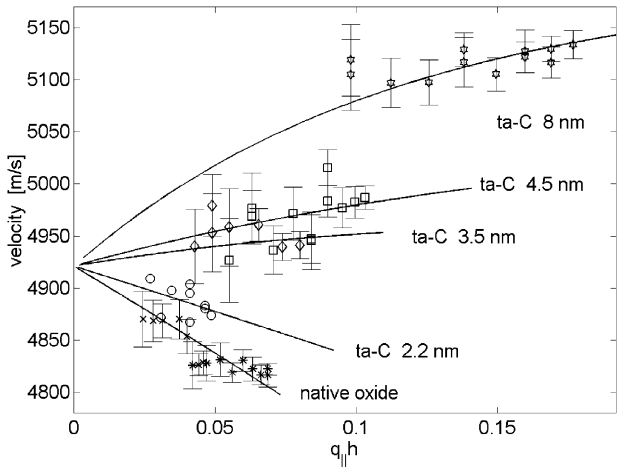

Fig. 2. Measured and computed dispersion relations for substrates A(*) and D(x), and samples of increasing thickness, B(□), C(▶), E(○) and F(◇), see Table 1. The error bars for sample E are not shown for clarity.

3.2. SBS

The Rayleigh wave (RW), the prototype of SAWS, has a wavevector $q_{\parallel}$ parallel to the surface, a velocity v_R independent from wavelength, and a displacement field which decays exponentially with depth, the decay length being the same as the wavelength $\lambda_{\parallel}=2\pi/q_{\parallel}$ [14]. If a layer of thickness h is deposited on a substrate, it modifies the spectrum of the substrate SAWs; the velocities become wavelength-dependent [15]. The RW becomes the modified Rayleigh wave (MRW), whose velocity is a function of $q_{\parallel}h$. Its displacement is mostly in the substrate. Close to the surface where the wave amplitude and energy density are maximum, the MRW propagates in the film and senses its properties. At higher values of $q_{\parallel}h$, the MRW is more confined in the film and more sensitive to its properties. Therefore, if the film is acoustically faster than the substrate, the MRW velocity is an increasing function of $q_{\parallel}h$, otherwise it is a decreasing function.

Spectra of SAWs can be measured by various techniques [3,4,16–18]. BS is the scattering of a photon by a long wavelength acoustic phonon. The scattering geometry selects the acoustic wavevector $q_{\parallel}$, and the velocity v_m is obtained from the measured frequency; $v_m=\omega/q_{\parallel}$. SBS measurements are time consuming, but the measurement is intrinsically contactless and local, and the probed acoustic wavelengths can be up to two orders of magnitude smaller than those probed by other techniques. This gives BS a unique potential for spatial resolution, particularly important for ultra thin films.

The elastic properties can be derived from the measured acoustic velocities. The velocities of SAWs in layered structures can be computed by the continuum elastodynamics equations as a function of the density and the elastic constants of the film and the substrate, and of h and $q_{\parallel}$ [14,19]. This gives the physical properties from measured SAW velocities, and the elastic constants are obtained fitting the computed velocities to the measured ones [6,20,21]. Amorphous films, being isotropic, have elastic constants completely determined by only two moduli such as the Young's modulus E, and shear modulus G. The data analysis gives a confidence region in the (E, G) plane and is supplemented by physical plausibility criteria. It is assumed that the carbon films have a positive Poisson's ratio ν, and a bulk modulus $B<B_{\text{diamond}}=445$ GPa. Only the part of the confidence regions satisfying these criteria gives the results.

The bare substrates were characterised by measuring the bulk phonons. The data agree with the accepted values for Si ($\rho=2.33$ g cm^{-3}, $C_{11}=166$ GPa, $C_{12}=63.9$ GPa, $C_{44}=79.6$ GPa, refractive index $n\sim4$). However, uncertainties in the measured velocities, result in a precision of at least 3%. SBS gave the dispersion relations of SAWs for the films (Fig. 2). Fig. 3 shows the 90–95–99% confidence regions in the (E, G) plane. The resulting E, G are reported in Table 1. The lines in Fig. 2 are computed from the most probable values of the (E, G) couple. The limit at $q_{\parallel}h=0$ is the Rayleigh velocity for a really bare Si substrate.

The data from the two native oxide films fall essentially on the same line, as expected. The dispersion relation for the oxide is a decreasing function of $q_{\parallel}h$, being acoustically slower than the substrate. The dispersion relation for the 2.2-nm carbon film is also decreasing, indicating that such a thin film is acoustically slower than the Si substrate, but stiffer than the native oxide. The data from the 3.5- and 4.5-nm carbon films fall approximately on the same curve. Their elastic constants are similar, and definitely higher than the 2.2-nm film. The dispersion relation is an increasing function

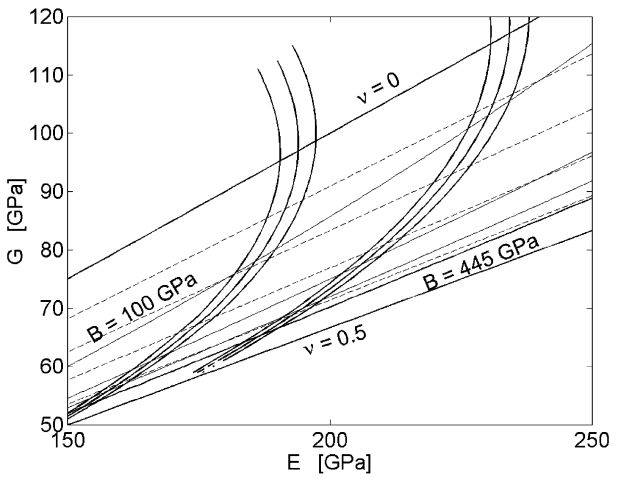

Fig. 3. 90–95–99% confidence regions for sample F, ~3.5 nm. The physical limits $\nu=0$, $\nu=0.5$ and $B=445$ GPa are shown. The continuous lines are $B=100$, 200 and 300 GPa; the dashed lines are $\nu=$ 0.1, 0.2, 0.3 and 0.4.

of $q_{\parallel}h$. The data from the 8-nm film fall on another definitely different curve, indicating a significantly higher stiffness as also shown by the elastic moduli, which begin to be comparable to those found for thicker ta-C films [6].

Since we are pushing both SBS and XRR to the limits, we wanted to be sure of the robustness of these results for slightly different values of the film properties. A 5% change in film density and/or thickness results in confidence regions which are largely overlapping, with mean values shifting by approximately 5%, but much less than the size of the confidence regions. This shows that our procedure is robust against inaccuracies [22]. However, a stronger sensitivity is found if the substrate properties change. If the substrate stiffness is under- or overestimated, the resulting change in the Rayleigh wave velocity would be attributed to the film, resulting in a corresponding over- or underestimation of film stiffness. This can introduce significant errors. Assuming Si elastic constants are ~1% lower gives ~30% higher elastic constants for the thinner films. The accuracy of the substrate stiffness is therefore crucial. We could test this since we measured the properties of films both slower and faster than the substrate. The dispersion relations of Fig. 2 were fitted by linear or quadratic functions, with the velocity at $q_{\parallel}h=0$ as a common fitting parameter for all the curves. The results indicate that the stiffness of the substrate might be slightly overestimated by <1%. This means that E and G of Table 1 might be slightly underestimated. Thus, the Young's moduli of the 8, 4.5, 3.5 and 2.2 nm films are at least ~380, 220, 200 and 100 GPa. According to the general E vs. sp^3 relation derived in ref. [6], the corresponding sp^3 contents would be ~60, 30, 20 and 0, and the corresponding densities from ref. [9], 2.7, 2.3, 2.2 and 1.9 g/cm^3. However, the average densities from XRR are ~2.8 g/cm^3, thus high also for the ultra-thin films, differently from what could be derived from the former relations derived for thick films. This shows that the ~8 nm marks the threshold for the films to behave like bulk ta-C, while for the thinner films in particular, the sub 4 nm films, the influence of the surface and interface layers make them softer than a corresponding bulk film of the same density and sp^3 content. A ~2.2 nm carbon film is made up of 10–20 carbon-atoms layers, and it is expected that it is softer than a corresponding 2.2 nm slice in a thicker ta-C film, due to the significant influence of the dangling bonds and lower density layers.

3.3. Raman spectroscopy

Fig. 4a,b,c compares the Raman spectra of the 4.5 nm-thick film deposited on Si and Si+Al for 514.5, 325 and 244 nm excitation. It is immediately evident how the addition of the thermally evaporated Al layer increases the measured Raman intensity by a factor ~2 for 514.5 nm excitation, ~40 for 325 nm excitation, and ~10 for 244 nm excitation. Indeed, the UV Raman spectra of the thinner film on Si are far too noisy to be analysed. This indicates that Al gives a surface enhancement of the Raman spectra (SERS), with a higher enhancement for high excitation energy. This is of interest since UV Raman spectra can directly probe the sp^3 content via the T peak at ~1050 cm^{-1} [23]. In the framework of the electromagnetic theory of surface enhanced Raman spectroscopy, the Raman intensity is enhanced by the coupling with the surface piasmon field of the metal [24,25]. The thermally evaporated Al is not a flat surface, but an assembly of blob-like and rod-like structures of 50–150-nm size, as seen by SEM. The surface plasmon for an Al flat surface or sphere coated by ta-C is 3.8–5.3 eV, considering the dielectric functions of both Al and ta-C [9,26]. This would explain the higher enhancement for higher excitation energy. This also explains the highest enhancement for 325 nm excitation, since this is ~3.82 eV and matches the surface plasmon energy of an Al sphere coated with ta-C. Indeed, we choose Al instead of the widely used Ag [24,25], in the hope of observing surface enhanced resonant Raman effects for UV excitation, due to the higher plasmon energy of Al [26]. Ag is suitable to selectively enhance low excitation wavelengths since the surface plasmon energy for ta-C coated Ag is in the visible–IR range. We thermally evaporated Al on Si, as this is a simple way to make a nanostructured substrate. Further work is in progress to achieve a better metal substrate, using also different metals, suitable to selectively enhance Raman spectra taken at the various excitation energies, in particular for 244 nm. This will be reported elsewhere together with a deeper discussion

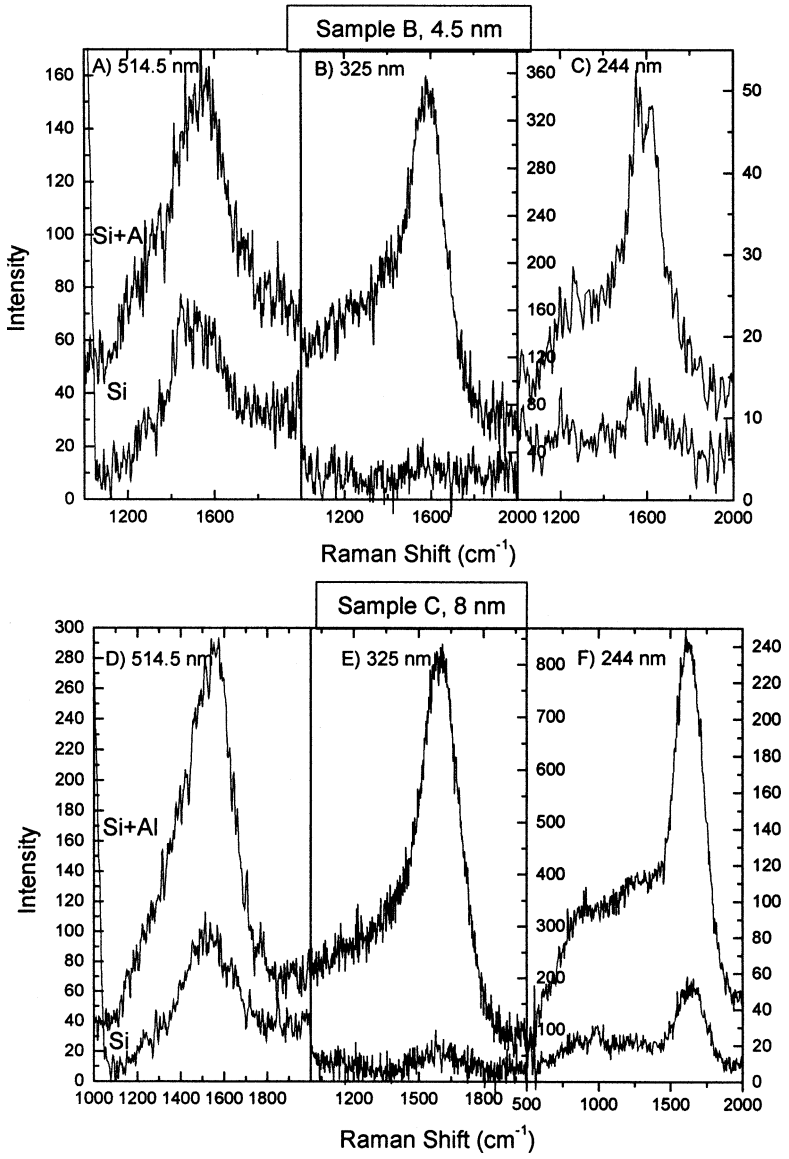

Fig. 4. (A,D) 514.5, (B,E) 325 and (C,F) 244 nm Raman spectra for samples B (~4.5 nm) and C (~8 nm) deposited on Si and Si+Al. The intensity for samples deposited on evaporated Al is higher at any excitation wavelength, the enhancement being bigger for UV Raman spectra (244 nm and especially 325 nm).

of SERS in DLCs. However, Fig. 4 shows that our simple approach is enough to allow a detection of UV Raman spectra of the same quality as thicker films, with no need to increase the power on the sample or the acquisition time.

The Raman spectra of all carbon systems consist of three features, approximately 1560, 1360 (for visible excitation) and 1060 cm^{-1} (detected only in UV excitation), which are labelled as the G, D and T peaks, respectively. The G and D peaks are due to sp^2 sites only. The G peak is due to the bond stretching of all pairs of sp^2 atoms in both rings and chains. The D peak is due to the breathing modes of sp^2 rings [27–29]. The T peak is due to C–C sp^3 vibrations. For a given substrate, if we compare the spectra of ultrathin films with the ones of thicker samples, we detect an increase of the G peak position ($1510 \rightarrow 1520 \rightarrow 1565$ cm^{-1} for the 2.2, 8 nm and bulk ta-C films), and an increase of $I(T)/I(G)$ ($0 \rightarrow 0.4 \rightarrow 0.5$) with thickness consistent with the lower sp^3 content and density of the thinner samples. The spectrum of the ~4.5 nm film shows less dispersion of the G peak with changing excitation energy (0.21 cm^{-1}/nm) than the 8-nm sample (0.45 cm^{-1}/nm, the same as bulk films), whose UV spectrum approaches the one of thicker ta-C films and has a significant $I(T)/I(G)$ ratio, consistent with high sp^3 content (>60–70%) [23,27–29], Fig. 4f. For a fixed thickness, if we compare the Raman spectra of samples on Si and Si+Al, we see

that films on Si + Al have a slightly higher $I(D)/I(G)$ ratio (0.1–0.2), lower G peak dispersion (max. = 0.35 cm^{-1}/nm) for varying excitation energy and lower $I(T)/I(G)$ ratio (max. = 0.35) than films grown on Si. This is consistent with the surface enhancement effect, which weights more the interface layer, which has a lower density and thus, higher sp^2 content. This difference could also be ascribed to a substrate effect, by which the nature of the films and interfaces is changing when depositing on Al or on Si and needs further investigation. In any case, this shows that the comparison of surface enhanced and normal Raman spectra allows to us probe the interface layers of the ultra-thin films, achieving a nanometre or sub-nanometre vertical resolution.

4. Conclusions

The combination of three non-destructive techniques of SBS, XRR and Raman spectroscopy was successfully applied to measure the density, thickness, roughness layering, sp^2 clustering, and sp^3 content for ultra-thin carbon films. An average density of ≥ 2.8 g/cm^3 is measured down to 2–3 nm thickness. The average elastic constants of the ultra-thin layers increase steeply with thickness, being comparable with those of thicker films already from 8 nm thick films. Even the thinnest 2.2 nm film has a Young's modulus of at least $\sim$100 GPa.

Acknowledgments

The authors thank D. Batchelder of Leeds University and M. Kuball of Bristol University for access to their UV Raman facilities. M.G.B and C.E.B. acknowledge financial support from Italian CNR — Progetto Finalizzato Materiali Speciali per Tecnologie Avanzate II. A.C.F acknowledges funding from an E.U. TMR Marie Curie research fellowship and from Churchill College, Cambridge.

References

[1] P.R. Goglia, J. Berkowitz, J. Hoehn, A. Xidis, L. Stover, Diamond Relat. Mater. 10 (2001) 271.
[2] J. Robertson, Thin Solid Films 383 (2001) 81.
[3] F. Nizzoli, J.R. Sandercock, in: G. Horton, A. Maradudin (Eds.), Dynamical Properties of Solids, North-Holland, Amsterdam, 1990, p. 281.
[4] P. Mutti, C.E. Bottani, G. Ghislotti, M.G. Beghi, G.A.D. Briggs, J.R. Sandercock, in: G. Briggs (Ed.), Advances in Acoustic Microscopy, vol. 1, Plenum, New York, 1995, p. 249.
[5] J.D. Comins, in: M. Levy, H.E. Bass, R.R. Stern (Eds.), Handbook of Elastic Properties of Solids, Liquids and Gases, Academic Press/Harcourt Publishers Ltd, Sidcup, UK, 2000, p. 349.
[6] A.C. Ferrari, J. Robertson, M.G. Beghi, C.E. Bottani, R. Ferulano, R. Pastorelli, Appl. Phys. Lett. 75 (1893) 1999.
[7] K.B.K. Teo, S.E. Rodil, J.T.H. Tsai, A.C. Ferrari, J. Robertson, W.I. Milne, J. Appl. Phys. 89 (2001) 3706.
[8] K.B.K. Teo, A.C. Ferrari, S.E. Rodil, J. Yuan, J.T.H. Tsai, J. Robertson, W.I. Milne, G. Fanchini, E. Tagliaferro, E. Laurenti, these proceedings.
[9] A.C. Ferrari, A. Li Bassi, B.K. Tanner, et al., Phys. Rev. B 61 (2000) 11089.
[10] S.K. Sinha, E.B. Sirota, S. Garoff, H.B. Stanley, Phys. Rev. B 38 (1988) 2973.
[11] M. Wormington, I. Pape, T.P.A. Hase, B.K. Tanner, D.K. Bowen, Phil. Mag. Lett. 74 (1996) 211.
[12] B.K. Tanner, A. Libassi, A.C. Ferrari, J. Robertson, Mater. Res. Soc. Symp. Proc. W11.4 (2001).
[13] C.A. Davis, K.M. Knowles, G.A.J. Amaratunga, Phys. Rev. Lett. 80 (1998) 3280.
[14] G.W. Farnell, in: W.P. Mason, R.N. Thurston (Eds.), Physical Acoustics, vol. 6, Academic Press, New York, 1970, p. 109.
[15] G.W. Farnell, E.L. Adler, in: W.P. Mason, R.N. Thurston (Eds.), Physical Acoustics, vol. 9, Academic Press, New York, 1972, p. 35.
[16] P. Zinin, in: M. Levy, H.E. Bass, R.R. Stern (Eds.), Handbook of Elastic Properties of Solids, Liquids and Gases, vol. 1, Academic Press/Harcourt Publishers Ltd, Sidcup, UK, 2000, pp. 187–226.
[17] D. Schneider, Th. Witke, Th. Schwarz, B. Schneich, B. Schultrich, Surf. Coating Technol. 126 (2000) 136.
[18] M.D. Whitfield, B. Audit, C.M. Flannery, L.P. Kehoe, G.M. Crean, R.B. Jackman, J. Appl. Phys. 88 (2000) 2984.
[19] A. Amici, M.G. Beghi, C.E. Bottani, Comp. Mater. Sci. 17 (2000) 404.
[20] M.G. Beghi, C.E. Bottani, P.M. Ossi, T. Lafford, B.K. Tanner, J. Appl. Phys. 81 (1997) 672.
[21] M.G. Beghi, C.E. Bottani, R. Pastorelli, in: C. Muhlstein, S.B. Brown (Eds.), Mechanical Properties of Structural Films, ASTM STP 1413, American Society for Testing and Materials, West Conshohocken, PA, USA, 2001.
[22] R. Pastorelli, S. Tarantola, M.G. Beghi, C.E. Bottani, A. Saltelli, Surf. Sci. 468 (2000) 37.
[23] K.W.R. Gilkes, S. Prawer, K.W. Nugent, et al., J. Appl. Phys. 87 (2000) 7283.
[24] M. Moskovits, Rev. Mod. Phys. 57 (1985) 783.
[25] F.J. Garcia-Vidal, J.B. Pendry, Phys. Rev. Lett. 77 (1996) 1163.
[26] R.F. Egerton, Electron Energy Loss Spectroscopy in the Electron Microscope, Plenum, New York, 1986.
[27] A.C. Ferrari, J. Robertson, Phys. Rev. B 61 (2000) 14095.
[28] A.C. Ferrari, J. Robertson, Phys. Rev. B 64 (2001) 075414.
[29] A.C. Ferrari, these proceedings.